Advances in Engineering Research : Possibilities and Challenges
ISSN Print: 3079-5192
ISSN Online: 3079-5206
https://doi.org/10.63313/AERpc.2017

Study on the Single-Pile Uplift Bearing Capacity Characteristics of Expanded-Disc Piles Based on FDM Numerical Simulation

YuNan Zhai
School of Civil Engineering, Lanzhou Jiaotong University, Lanzhaou, 730070, China
Email: zyn129013@163.com

How to cite this paper: Zhai, Y. N. (2026). Study on the single-pile uplift bearing capacity characteristics of expanded-disc piles based on FDM numerical simulation. *Advances in Engineering Research: Possibilities and Challenges*, 3(3), 1–10. ISSN Print: 3079-5192; ISSN Online: 3079-5206.
https://doi.org/10.63313/AERpc.2017
Published: 2026-03-06

Copyright © 2026 by author(s) and Erytis Publishing Limited.
This work is licensed under the Creative Commons Attribution International License (CC BY 4.0).
http://creativecommons.org/licenses/by/4.0/



Abstract

Concrete enlarged-head piles, as a novel variable-section pile type, exhibit significantly superior bearing capacity compared to conventional straight-bore piles. To systematically investigate the influence of enlarged-head quantity on vertical uplift bearing capacity, this study employs a combined approach of laboratory model testing and numerical simulation. Finite Difference Mesh (FDM) models were established for straight-bore piles, single-enlarged-head piles, and double-enlarged-head piles to elucidate their mechanical behavior. Results indicate: Computational outcomes from the numerical simulation method demonstrate excellent consistency with model testing, validating the reliability of simulated results. The enlarged-head structure exhibits a markedly significant enhancement effect on pile foundation uplift bearing capacity, with the ultimate bearing capacity of single-head and double-head piles reaching 1.5 times and 2.5 times that of straight-bore piles respectively, highlighting the more pronounced strengthening effect of the double-head configuration. Under ultimate conditions, the shear slip planes of the upper and lower discs interconnect to form a continuous composite failure surface, fully utilizing the shear strength of both inter-disc and disc-top soils. In summary, the finite difference numerical model accurately replicates the complex interaction mechanisms between pile foundations and soil, providing reliable technical support for studying pile-soil interaction principles and quantifying the soil reinforcement zone around enlarged-disc piles.

Keywords

Expanded pile; Laboratory testing; FDM numerical simulation; Pile-soil interaction; Bearing characteristics

1. Introduction

Pile foundations represent the most widely employed form of building foundation within the engineering sector. With the continuous advancement of geotechnical engineering techniques, both the theoretical underpinnings and construction

methodologies associated with pile foundations have reached a high degree of maturity. The concrete enlarged-end pile (CEP) constitutes a novel type of variable-section cast-in-place pile. This specialized pile design incorporates locally enlarged sections within the conventional cast-in-place pile body, thereby increasing the resistance at the enlarged end and enhancing bearing capacity. Compared to conventional straight-bore cast-in-place piles, CEPs offer significant advantages including enhanced bearing capacity, reduced settlement, effective pile length reduction, lower construction costs, and mature construction techniques. Consequently, they have gained extensive application in large-scale building foundation projects. Currently, scholars have conducted extensive research on the macro-failure behavior of concrete enlarged-diameter piles under single-pile, double-pile, and pile-group conditions, alongside their engineering applications. However, existing studies lack systematic comparisons between the failure mechanisms of CEP piles and straight-bore piles, and a comprehensive theoretical framework for their failure effects remains incomplete. This deficiency in theoretical research has, to some extent, constrained the further promotion and optimized application of CEP pile technology. Therefore, undertaking systematic research into the failure behavior of single CEP piles, combined with macro-micro numerical analysis methods to deeply elucidate their failure mechanisms, holds significant theoretical value and practical engineering significance.

Over the past decade, the development of enlarged-head piles has yielded a wealth of research findings[1]. Through field and model testing, scholars have investigated the vertical bearing capacity of enlarged-head piles and piles of uniform diameter using in-situ static load tests. These studies have explored the load-bearing performance, load transfer patterns, and pile-soil interaction mechanisms of enlarged-head piles. To further analyze the influence of enlarged pile geometric parameters on vertical compression resistance, uplift resistance, horizontal bearing capacity, and surrounding soil failure patterns, some researchers have employed model tests to investigate the effects of factors such as disc cross-sectional shape, disc diameter, disc spacing, and number of discs on bearing capacity[2,3]. This experimental approach is relatively costly and can only assess the force transfer process, failing to measure displacement at the pile-soil interface or variations in the stress field.

To overcome the limitations of conventional testing, modern research employs advanced techniques such as Digital Image Correlation (DIC) to provide a more comprehensive understanding of pile-soil interactions[4]. Xu Lina et al. conducted dynamic continuous monitoring of the failure patterns and displacement changes in the soil surrounding piles using a half-pile model test with in situ soil, combined with Digital Image Correlation (DIC) and non-contact full-field strain monitoring equipment (VIC-3D). They investigated the effects of enlarged diameter and spacing on the pull-out resistance characteristics of enlarged-diameter piles under vertical

loading. Nevertheless, the mechanism governing load transfer at the pile-soil interface warrants further investigation.

To address the limitations inherent in physical experiments, scholars both domestically and internationally have employed finite element numerical analysis to investigate the load transfer mechanisms and surrounding soil failure patterns of enlarged-head piles. Xie Hongli et al. employed Abaqus finite element software to investigate the axial force transfer patterns, lateral friction distribution characteristics, end resistance evolution mechanisms, and settlement deformation features of expanded-base piles. They further examined the pile length optimization mechanism and stress distribution principles for such piles. Li et al.[5] examined the bearing behavior of CEP piles versus straight piles based on field tests and FLAC3D numerical simulations, investigating how the position, number, dimensions, and spacing of enlarged discs influence CEP pile performance. However, current finite element simulation techniques, while providing effective analysis at the macroscale, remain inadequate for precisely characterizing soil particle displacement and load transfer mechanisms at the pile-soil interface from a micro-scale perspective.

Therefore, to investigate the uplift bearing capacity and soil failure effects around enlarged-head piles in greater depth, this study employs the Finite Difference Mesh (FDM) numerical coupling method based on laboratory tests of enlarged-base piles. Numerical simulations of uplift bearing capacity were conducted for three pile types: straight piles, single-disk enlarged-base piles, and double-disk enlarged-base piles. This approach reveals, at a macro level, the mechanical behavior of enlarged-base piles under vertical uplift loads and the soil failure effects around the piles. The findings provide reliable technical support for investigating pile-soil interactions and determining the effective soil reinforcement zone around enlarged-head piles.

2. Materials and methods

2.1. Test apparatus and model preparation

This study employs a small-scale indoor model testing method, with the test model box dimensions being 0.6 m (length) × 0.6 m (width) × 1.2 m (height). The model chamber was fabricated from angle steel and steel plates, welded to provide adequate boundary constraints. The loading system comprised a reaction frame, displacement dial gauges, hydraulic jacks, and load cells. In actual engineering practice, concrete spreader-plate piles are formed by concrete casting. However, in model testing, the size effect of concrete aggregates significantly impacts pile formation quality. Therefore, acrylic was employed as the pile material in this model. During testing, vertical loads were applied via the hydraulic jack, with load sensors providing real-time monitoring and control of pile-head load magnitude. Pile-head settlement was measured using dial gauges, while axial forces along the pile shaft were monitored via strain gauges affixed to the structure. The experimental apparatus is illustrated in Figure 1.

Figure 1. Experimental apparatus



The test soil was sourced from aeolian sand in the heart of the Tengger Desert. The control fill soil was maintained at an optimum moisture content of wop=13.5%, with a compaction coefficient K=0.90, maximum dry density ρd=1.73 g/cm^3, cohesion c=3.5 kPa, and internal friction angle φs=31.6°. The model pile measured 900 mm in length with a diameter of 40 mm. The bearing disc featured a diameter of 80 mm and a height of 32.5 mm, with the model pile embedded 800 mm into the soil. The dimensions and disc positions for the straight-hole pile, single-disc pile, and double-disc pile are shown in Figure 2. To monitor pile body strain under vertical loading, fourteen strain gauges were symmetrically arranged on the model pile surface at 100 mm intervals. Following strain gauge application, the pile surface was uniformly coated with epoxy resin and standard sand was evenly distributed to enhance surface roughness, as illustrated in Figure 3. Model construction commenced by laying a 20cm thick wind-deposited sand foundation at the base of the model box. The model pile was then positioned centrally within the box and filled in layers using a layered compaction technique, with each fill layer controlled to a thickness of 15cm.

The vertical load test was conducted in accordance with the methodology outlined in the literature, employing a hydraulic jack to apply loads using the slow-load maintenance method. Straight piles were loaded incrementally in 200 N steps, while single-disc and double-disc piles were loaded incrementally in 500 N steps respectively. When a distinct inflection point appeared on the pile load-settlement curve, or when settlement exceeded 80 millimeters, the pile was deemed to have reached its ultimate equilibrium state, at which point loading ceased.

Figure 2. Schematic diagram of the model pile



2.2. Finite Difference Model Development and Simulation

Finite difference numerical simulations of indoor model tests were conducted using FLAC^{3D} finite difference software. This numerical simulation employed data from laboratory model tests, with a pile length of 900 mm and an embedded length of 800 mm. Along the pile shaft, 0, 1, or 2 load-bearing discs were positioned, each with a diameter of 80 mm and a pile diameter of 40 mm. The computational domain surrounding the pile matched the dimensions of the model box, with the soil layer beneath the pile toe measuring 400 mm in height. The origin of the model coordinate axes was positioned at the center of the soil base, with the Z-axis oriented parallel to the pile axis and directed upwards. Contact surfaces between the pile and soil were generated using the INTERFACE command, permitting sliding or separation. The stepwise loading sequence and load levels were refined based on the laboratory model test data. The finite difference model is illustrated in Figure 3.

The pile body in the model employs a homogeneous continuous linear elastic constitutive model; the surrounding soil adopts an MC constitutive relationship, assuming it to be a homogeneous, continuous, isotropic, ideal elastoplastic material. The model constrains normal deformation around its perimeter and constrains deformation in all directions at its base. The material parameters for the model are presented in Table 1.

In the formula, K denotes the volumetric modulus, G represents the shear modulus; $\triangle_{zmin}$ signifies the minimum contact width in the normal direction of the contact surface; the maximum value notation indicates that the maximum value from all adjacent regions at the interface should be adopted; the friction and cohesion forces at the contact surface are determined according to soil properties. The characteristics of the contact surface between the pile body and soil are shown in Table 2.

Figure 3. Finite difference mesh of the pile

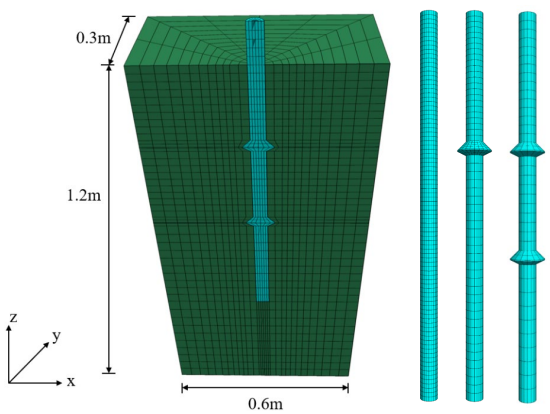


Table 1. Pile–soil parameter assignment

Materials	ρ/(kg·m^{-3})	E/MPa	μ	c/kPa	φ/°

Pile body	2400	6.9×10^4	0.20	—	—
Aeolian sand	1688	8	0.35	0	35

Table 2. Material properties of the pile–soil interface

k_n/Pa.m^{-1}	k_s/Pa.m^{-1}	c/kPa	φ/°
1.78×10^7	1.78×10^7	0	15.9

In numerical simulations, the soil mass is first allowed to achieve initial stress equilibrium under its own weight. The pile installation is then simulated using the 'element replacement method': soil elements at the pile location are removed, and a pile model is generated at the corresponding position with assigned material parameters, until the model reaches a new equilibrium state. Once the pile installation has stabilized, the initial displacement field of the soil is reset to zero to eliminate displacement history induced by the installation process. Finally, a vertical load is applied to the pile cap to calculate the compressive bearing capacity. By simulating the single-pile compression process using the aforementioned parameters and workflow, key response data such as pile cap displacement, pile body stress, and strain can be obtained.

3. Results

(1) Load-Settlement Analysis

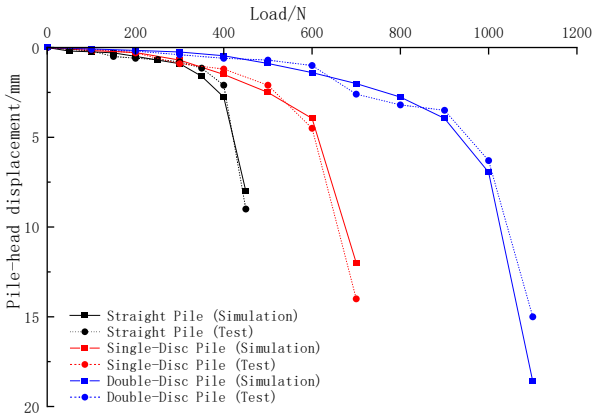
Figure 3 presents the numerical simulation versus laboratory test comparison of load-displacement (Q-s) curves for straight-bore piles, single-ring piles, and double-ring piles under uplift loading. The figure demonstrates that the Q-s curves for all three pile types exhibit abrupt transitions with distinct steep-decline segments. As the load increases incrementally, the uplift displacement at the pile head correspondingly increases. At the same load level, the double-disk pile exhibits the smallest uplift displacement, the straight-bore pile the largest, and the single-disk pile an intermediate value. Test results indicate that the ultimate uplift bearing capacities for the straight-bore pile, single-disk pile, and double-disk pile are 400 N, 600 N, and 1000 N respectively. Compared to straight-bore piles, the ultimate uplift bearing capacities of single-disk and double-disk piles increased by 50% and 150% respectively, indicating that the disk-expansion structure still delivers significant load-enhancing effects under uplift conditions.

The pull-out Q-s curve exhibits distinct displacement discontinuities, with straight-bore piles showing a rapid decline in bearing capacity after reaching peak values, whereas the decline in the latter half of the enlarged-base pile curve is more gradual, demonstrating superior ductility. Mechanistically, the pull-out resistance of straight-bore piles relies entirely on pile-soil interface friction. Once the peak static friction is exceeded, dynamic friction struggles to sustain high loads. Conversely, the pull-out resistance of enlarged-base piles primarily originates from the self-weight of the soil above the enlarged base and its shear resistance. Numerical results indicate that the ultimate pull-out resistance of double-disk piles reaches 2.5 times that of

straight-bore piles, further demonstrating that optimizing the structure to mobilize soil shear strength is an effective approach to enhancing pull-out performance.

Moreover, the numerical simulations exhibit good overall agreement with the Q-s curves obtained from laboratory tests, particularly demonstrating high consistency in the load-displacement behavior. This result validates the reliability of the pile-soil numerical model established using FLAC3D under uplift conditions, confirming its capability to accurately reflect the mechanical response characteristics of enlarged-head piles subjected to vertical uplift loads.

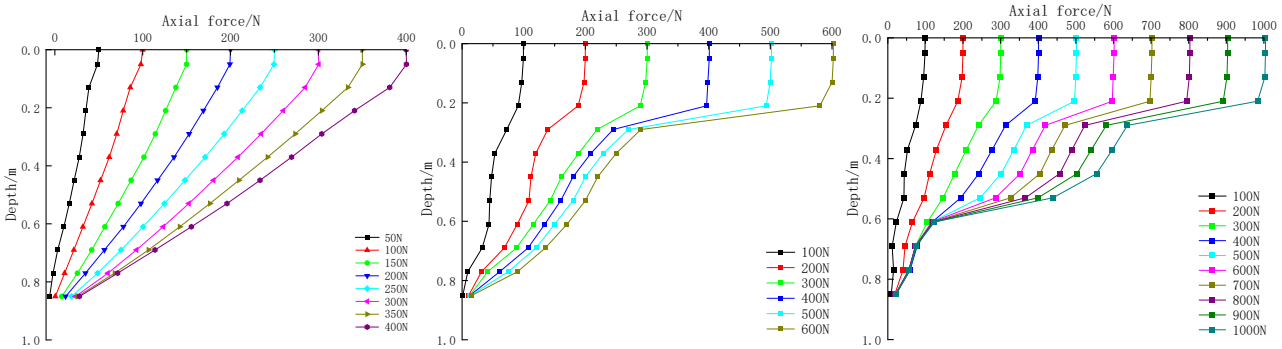
Figure 4. Q–s curves of the three pile types



(2) Analysis of Axial Force Transmission in Piles

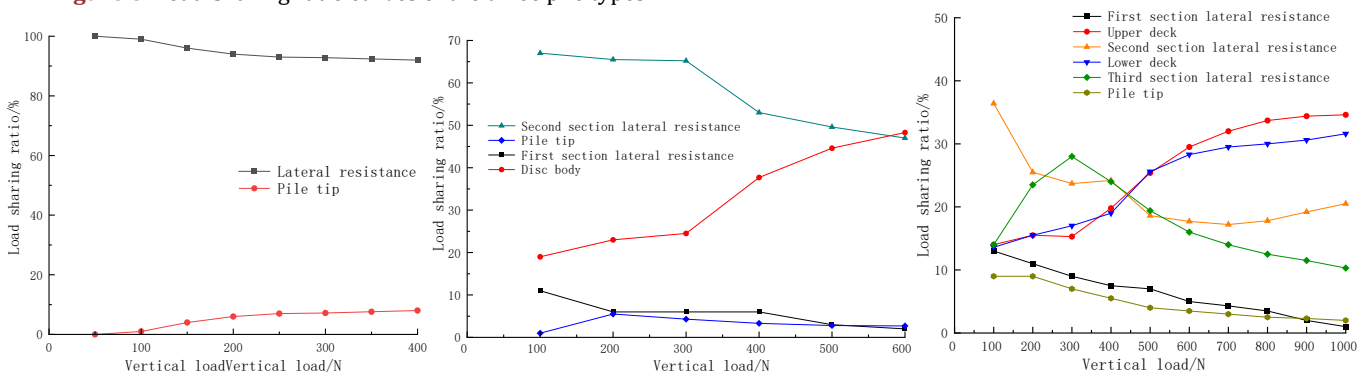
Figure 5 illustrates the axial force distribution within the pile body for straight-hole piles, single-disk piles, and double-disk piles under various load levels. Figure 6 presents the load-sharing ratio curves for the three pile types. The figures reveal that as the pile-head load increases, axial force progressively rises across all cross-sections of the three pile types, exhibiting a gradual attenuation trend with increasing depth. This indicates that the load is progressively transferred to the surrounding soil through lateral friction resistance, pile-end resistance, and enlarged-disk resistance. The slope of the axial force curve directly reflects the magnitude of axial force variation within the pile body. For straight-bore piles, lateral friction resistance is largely fully utilized at low loads. As loads increase further, lateral friction resistance stabilizes while the proportion of load borne by the pile tip gradually decreases. At ultimate load, the pile tip load-sharing ratio reaches 10%, with the remainder borne by the pile side. Both single-flange and double-flange piles exhibit a pronounced attenuation trend in axial force curves at each flange location. Each additional flange layer significantly reduces axial force within the pile body. This demonstrates that the flanges effectively share part of the load through their end-supporting action, altering the load transfer path at the flange locations. At ultimate load conditions, the enlarged disc of the single-disc pile bore 48% of the load, with the pile tip bearing 3% of the load share; for the double-disc pile, the upper disc bore 33% of the load and the lower disc bore 31%, with the pile tip bearing 2% of the load share.

Figure 5. Axial force distributions of the three pile types



(a)Straight-bore pile (b)Single-disc enlargement pile (c)Double-disc enlargement pile

Figure 6. Load-sharing ratio curves of the three pile types



(a)Straight-bore pile (b)Single-disc enlargement pile (c)Double-disc enlargement pile

(3) Displacement Field Analysis

Figure 7 presents the vertical displacement contour plots for the three pile types at ultimate bearing capacity. Under ultimate loading, straight-bore piles exhibit overall uplift. Displacement of the surrounding soil is concentrated near the pile side, rapidly diminishing with increasing distance from the pile. High-displacement zones form elongated, narrow bands distributed along the pile body, indicating a failure mode characterized by localized shear slip at the pile side. This failure does not propagate to the ground surface to form an overall wedge-shaped failure zone.

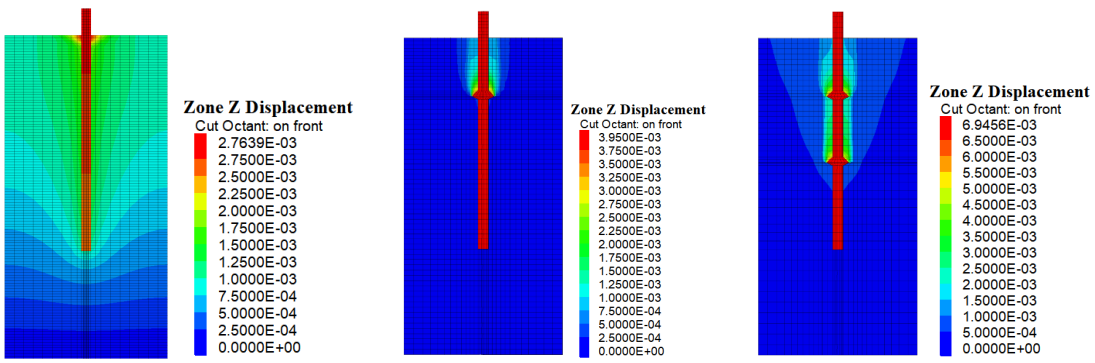
The displacement distribution of single-disk piles differs markedly from that of straight-bore piles: a distinct zone of high displacement concentration forms near the pile disk. A plastic shear zone first develops at the disk rim, subsequently extending from the disk edge towards the ground surface at an inclination of approximately 45° + φ/2, forming an inverted conical failure surface. The overall uplift of the soil mass above the enlarged pile cap indicates a pronounced tensile effect exerted by the cap structure on the overlying soil, while displacement beneath the enlarged cap remains relatively minor.

The failure pattern of double-disk piles is more complex: it manifests as an integrated composite shear block formed by the synergistic action of the upper and lower disks.

The shear plane initiated by the lower disk extends upward to terminate at the base of the upper disk, while the upper disk continues to develop new slip planes. Upon interconnecting, these form a large-volume failure body combining a cylindrical section (inter-disk soil) with an inverted conical section (soil above the upper disk). Significant high-displacement zones appear near both upper and lower discs, with the inter-disc soil mass cooperatively uplifted, rendering the entire failure contour as a complete inverted cone. This failure pattern indicates that the uplift resistance capacity of double-disc piles is not a simple summation of single-disc capacities. Its load-bearing mechanism involves stress redistribution and interaction within the inter-disc soil mass, validating the criticality of the critical inter-disc spacing in pile foundation design.

In summary, the pile configuration exerts a significant influence on the pull-out failure mode: straight-bore piles exhibit a smaller failure zone, with slip planes distributed nearly parallel to the pile side; single-disk piles, owing to the presence of the expansion disk, see the failure zone extend onto and around the disk, forming inclined slip planes; double-disk piles, through the synergistic effect of multiple disks, facilitate a larger-scale, integrated failure, with continuous and intact slip planes. As pile types evolve from straight-bore to multi-disk configurations, uplift failure progressively shifts from localized shear slip to holistic uplift failure. The pile-disk structure not only enhances bearing capacity but also markedly alters the failure mechanism within the pile-soil system.

Figure 7. Pile–soil displacement contour plot



(a)Straight-bore pile(400N) (b)Single-disc enlargement pile(600N) (c)Double-disc enlargement pile(1000N)

4. Conclusion

(1) The load-displacement curves from indoor model tests and finite difference method (FDM) numerical simulations showed a high degree of agreement, demonstrating the FDM's exceptional reliability and accuracy in simulating the complex interaction between enlarged-base piles and surrounding soil.

(2) The presence of the enlarged base significantly enhances the vertical uplift bearing capacity of the pile foundation. Compared to straight-bore piles, the bearing capacity of single-enlarged-base piles and double-enlarged-base piles increased by

50% and 150% respectively.

(3) Displacement contour plots reveal that the failure mode of enlarged-base piles shifts from shear slip along the pile-soil interface in straight-bore piles to predominantly shear failure of the inverted conical soil mass. At ultimate load, the shear planes initiated by the upper and lower discs in double-disc piles interconnect, forming a continuous composite failure surface combining columnar and inverted conical zones. This fully utilizes the self-weight and shear strength of the soil across both discs and the surrounding area. This 'dual-disc synergy' effect is the primary reason for the 2.5-fold increase in uplift bearing capacity compared to straight-bore piles.

References

[1] Rizwan M, Naseem S, Tarar M A.Soil-structure interaction and uplift bearing capacity: A study on low-header CEP single pile foundations[J].Physics and Chemistry of the Earth,2026, 142: 104255–104255.

[2] Qian Y, Li Y, Wang X, et al.Influence of Pile Spacing on the Compressive Performance and Soil Failure Mechanism of CEP Double Piles[J].Infrastructures,2025, 10 (11): 297–297.

[3] Qian Y, Li H, Tian W, et al.Effect of Pile Spacing on Load Bearing Performance of NT-CEP Pile Group Foundation[J].Buildings,2025, 15 (9): 1404–1404.

[4] Lina X, Haoyun D, Lei N, et al.Study on Soil Displacement Fields around the Expanded Body of Drill-Expanded Concrete Piles Based on DIC Technique[J].Applied Sciences,2021, 11 (19): 9097–9097.

[5] Ting L, Peng X, Guangqing Y.Investigation into bearing performance of concrete expanded-plates piles: Field test and numerical modelling[J].Engineering Structures,2022, 271.